



Article

Comparative Study on the Energetic and Ecologic Parameters of Dual Fuels (Diesel–NG and HVO–Biogas) and Conventional Diesel Fuel in a CI Engine

Alfredas Rimkus , Saulius Stravinskas and Jonas Matijošius * 

Department of Automobile Engineering, Faculty of Transport Engineering, Vilnius Gediminas Technical University, J. Basanavičiaus Str. 28, LT-03224 Vilnius, Lithuania; alfredas.rimkus@vgtu.lt (A.R.); saulius.stravinskas@vgtu.lt (S.S.)

* Correspondence: jonas.matijosius@vgtu.lt; Tel.: +370-684-041-69

Received: 10 December 2019; Accepted: 31 December 2019; Published: 3 January 2020



Abstract: The Article presents the results of the experimental research and numerical analysis of a compression ignition (CI) engine adapted for running on dual fuels of different composition (diesel and natural gas, diesel and biogas, biodiesel and natural gas, and biodiesel and biogas). The main goal was to find out the impact of different dual fuels on energy performance and emissions depending on the start of injection (SOI) of diesel and the crank angle degree (CAD). Pure conventional diesel fuel and second generation hydrotreated vegetable oil (HVO) (Neste) was used in the research. Natural gas contained 97 vol. % of methane. Biogas (biomethane) was simulated using a methane and carbon dioxide blend consisting of 60 vol. % of methane and 40 vol. % of carbon dioxide. Dual (liquid and gaseous) fuels were used in the tests, with the energy share of liquid fuels accounting for 40% and gas for 60%. The research results have shown that having replaced conventional diesel fuel with dual fuel, engine's BTE declined by 11.9–16.5%. The use of methane in the dual fuel blend reduced CO₂ volumetric fraction in the exhaust gases by 17–20%, while biomethane increased CO₂ volumetric fraction by 10–14%. Dual fuel significantly increased CO and HC emissions, but NO_x volumetric fraction decreased by 67–82% and smoke by 23–39%. The numerical analysis of the combustion process revealed changes in the ROHR (Rate of Heat Release) that affected engine efficiency and exhaust emissions was done by AVL (*Anstalt für Verbrennungskraftmaschinen List*) BOOST program.

Keywords: biogas; biodiesel; pollutant emissions; engine efficiency; rate of heat release

1. Introduction

The use of biogas over recent decades has been considered an intermediate step in the present oil industry shifting towards the production of alternative fuels. Thus, the aim of the European Union to strengthen research initiatives has become a trend in the pursuit of promoting the use of biogas in industry and for public needs [1], and the development of biogas production has spread across Europe since the end of the last century. This has been encouraged by the transposition of European Union directives into the national law. There has also been a shift in the reasoning behind biogas production from energy independence, bio-manure, and slurry processing to green energy resource production in order to reduce CO₂ emissions [2,3]. This trend has become global. China, with its annual theoretical biogas output of 73.6 billion m³ is one of the countries developing biogas production the fastest [4], while Indonesia can generate about 9597.4 billion m³ of biowaste per year alone [5]. Anaerobic digestion is also used to produce biogas, using a variety of raw materials of biological origin [6]. Accordingly, biogas production often faces the problem of underdeveloped technologies,

which reduces the profitability of biogas production and use, which in turn reduces the enthusiasm for its use [7]. Therefore, in order to receive support through funding and financing of new research in this field, continuously rationalizing biogas production technologies that enhance the attractiveness of the use of biogas itself is necessary [8]. Such biogas development must be focused on sustainability so that every part of the biogas life cycle is integrated with its neighboring component, from production to use [9]. Thus, laws of a circular economy offer using biogas resources not only for heat [10] and electricity production, but also in transportation as an alternative to fossil fuels [11]. Using biogas as a fuel for internal combustion engines allows one to also use it in vehicles and stationary cogeneration power plants, which use a diesel generator to produce electricity [12]. However, even though supported by respective regulations and directives, the transport sector does not use biogas resources that quickly. This is due to a poor development of production technologies and biogas as fuel in the network [13]. Small regional biogas plants have been offered as an alternative to biogas stations, as they could not only produce biogas, but to also sell it [14]. However, given stringent requirements which the quality of fuel is subject to, this option has been rejected [15]. Another method of use of biogas is its possible conversion into biomethane (third generation biofuel) and its use in fuel cells [16]. Thus, the use of biomethane as a vehicle fuel has been limited and solely in the areas where it was subsidized and where installing respective technologies was possible [17]. Stockholm's transportation system, where solutions of the use of biogas have played an important role, could be one such example. A long-term development has created well-functioning social and technical systems that include cooperation. However, the uncertainty as to the demand and policies has given rise to hesitation and signs of stagnation in the development [18]. Growing environmental pollution and limited fossil fuel reserves have encouraged research of the use of alternative renewable fuels for internal combustion engines [19].

Having made the necessary changes to the engine power system, natural and biogas may be used as a renewable energy source in internal combustion engines [20–23]. Supplying biogas reduces the thermal efficiency of both spark ignition (SI) and compression ignition (CI) engines. However, the engine operating in HCCI (Homogeneous charge compression ignition) mode indicates that the thermal efficiency is close to that of diesel engines [24]. Using dual fuel system, where other fuels are also supplied along with biogas and natural gas, has been offered as an alternative [25]. The use of such a system allows achievement of the goals set through the use of alternative fuels and pollution reduction, at the same time analyzing them more intensively for the specifics of the engine's operating process [26–29]. Various injection strategies have been used to analyze the use of natural gas/diesel blends in compression ignition engines [30]. Diesel engines can be modified so that natural gas inside the intake manifold is fumigated [31]. The time of injection of diesel and the proportion of natural gas have a major impact on the combustion mechanism, and this impact becomes even more evident at partial loads [32]. The mixed natural gas combustion stage can be improved by using a slower natural gas injection time [33]. The use of a dual injection strategy at the maximum pressure allows achieving thermal efficiency of more than 45% and limiting NO_x emissions. When using a single injection strategy, thermal efficiency is more than 45% with the engine operating in the range of low and medium loads, and a mere 35.5% at high loads, which can be explained by higher combustion losses [34]. With the engine operating at low loads and using various injection strategies, the combustion of dual fuel (natural gas and diesel blend) can be improved by a lower diesel start of injection (SOI) and a greater opening of the EGR (Exhaust gas recirculation) valve [35]. Increasing injection pressure significantly reduces the amount of unburnt methane in dual fuel engines with split injection. However, with methane concentration having reached 65%, the injection pressure has an impact on emissions of unburnt methane [36]. The amount of unburnt methane may form due to the temperature being too low at the cylinder wall, but increasing the injection pressure will increase the speed of methane flame propagation. Peroxide compounds have been found to have a significant influence on the combustion temperature during combustion of natural gas and diesel blends [37]. Correspondingly, slightly opening the EGR reduces the amount of unburnt methane, however, an increase of the degree of the opening of EGR proportionately increases methane content [38]. With increasing the amount of

natural gas in the blend, the curves of the speed of heat emission have one peak only initially, then turn into two peaks, and finally changing to a nearly single peak [39]. Zhang et al. [40] claimed that with the natural gas concentration having reached 55% and above, the combustion process deteriorates, even though the calculations show that the combustion process is normal supplying gas at 0 to 60%. The respective use of the NSGA-II (Nondominated sorting genetic algorithm) optimization algorithm allows optimizing such parameters as the gas spray angle and the time frame between the spray of diesel and gas [41]. The supply of natural gas and diesel blends to a rotary engine revealed that the combustion process occurs at the front and the middle of the combustion chamber. The total speed of fuel combustion improved having increased the amount of natural gas supplied, which in turn led to an increased rate of flame propagation. Compared to diesel, supplying up to an additional 20% of natural gas increased the maximum combustion pressure by ~24% [42]. In the event of an auxiliary ignition, natural gas accumulates at the end of the combustion chamber and diesel at its front and middle, and when delaying the injection time, the blend itself becomes more concentrated due to a shorter mixing period [42]. When changing the injection time, the maximum cylinder pressure correlates with the second peak of the speed of heat release, while having extended the shape of the injection nozzle by 2 cm, the combustion process deteriorates also increasing pollutant emissions [43]. The use of *Jatropha* biodiesel and biogas blends has shown that the CO₂ content of the biogas does not affect the thermal efficiency of the engine. As a result, the lowest quality of biogas (60% carbon dioxide) releases about 30% methane heat compared to 80% pure methane [44]. Oxygenated additives (papaya seed oil biodiesel blended with diglyme, butanol, and stone fruit biodiesel) can be a viable way to effectively use biodiesel blends in a diesel engine [45]. The engine's best features were stone biodiesel and papaya seed oil [46]. However, further research into tribological efficiency analysis is needed to make this ternary blend a future alternative energy source on a commercial scale [45]. This type of biodiesel (papaya-*Carica papaya*) complied with both ASTM (American Society for Testing and Materials) and EN (European Union) biofuel standards [47]. However, before recommending commercially available papaya seed biodiesel as an alternative source of energy, additional research is needed on engine emissions, cylinder pressure, burning rate data, combustion analysis, and tribological performance analysis [48].

Similar trends have also been observed in the analysis of the use of biogas and diesel blends in internal combustion engines. Biogas and natural gas are predominantly made up of methane with its higher content in natural gas [5]. A homogeneous mixture of biogas and air significantly increases the pressure in the engine cylinders [49]. Feroskhan et al. [50] noticed that with the engine operating at low loads, biogas provided up to 90% of energy required for engine's operation. When increasing the compression ratio from 16.5 to 19.5, a biogas and diesel-fuelled engine ran smoother and emitted less exhaust gas. At the same time, adjusting the EGR valve reduced engine efficiency, which manifested at high engine loads in particular [51], because the increasing EGR flow slows down the combustion phase, prolonging the ignition time [52]. Rahman and Ramesh [53] observed that when increasing the biogas content from 24% to 68%, the ignition delay decreased and the speed of combustion increased, thus, in order to stabilize the two indicators, advancing the start of diesel injection by three crank angle degrees (CADs) was proposed. The operation of dual fuel at the injection timing of 26 CAD BTDC (Before Top Dead Center) rendered a better overall result than other injection times [54]. Biogas was observed to be able to significantly reduce diesel consumption, thus, the diesel replacement ratio ranged from 15% to 88% in the present compression ignition engines. On the other hand, thermal engine efficiency is significantly affected by methane concentration and the flow of biogas, while the maximum thermal efficiency is achieved at the optimal biogas flow [55]. Sarkar and Saha [56] determined that the maximum threshold for the replacement of diesel with biogas was 92.49% and 97.55% depending on the load of a compression ignition engine. A further increase of the amount of biogas drastically reduced the engine efficiency coefficient. When comparing an engine fuelled on dual fuel (biogas and diesel fuelled compression ignition engine) and on biogas only, Mohamed et al. [57] observed that the latter engine had a better thermal efficiency and a lower pollution. The use of

biogas (i.e., having decreased methane concentration and increased CO₂ concentration compared to natural gas) allows increasing the Brake Mean Effective Pressure (BMEP) from 4 to 5 bars. Moreover, a lower CH₄ (i.e., an increased share of CO₂) also allowed using delayed SOI for diesel, which led to reduced smoke emissions [58]. Unrefined biogas can also be used in biodiesel-powered diesel engines in dual fuel mode. However, reducing CO and HC (Hydrocarbons) emissions is also needed by using appropriate techniques [59]. Both natural gas and biogas and fuel blends with diesel allowed achieving better environmental indicators. The more homogeneous the blend is, the more the values of particulate matter/smoke drops. On the other hand, HC and CO emissions increased due to varying reactivity of fuel components, also increasing NO_x emissions, especially at low engine loads [4,6,49,52,54,55,58]. The use of biogas containing up to 73% methane yields a significant ecological effect on engine life from *P. pinnata* plant biomass. Their use reduces NO, CO₂, and smoke by 39%, 42%, and 49%, respectively, using a 0.9 kg/h biogas stream. This results in a corresponding reduction in diesel fuel consumption of 0.215 kg/h [60].

With the dual fuel system and engine compression ratio at 18, diesel fuel consumption can be reduced to a maximum of 79.46%. Increasing the compression ratio from 16 to 18 can achieve the ecological effect: 41.97% for HC and 26.22% for CO [61]. Similar reductions in diesel fuel consumption are also observed with industrial dual fuel engines in the fertilizer granulation process. The effect observed was up to 63% replacement of diesel with natural gas [62].

The biogas mixing ratio in the mixing chamber and the dimethyl ether (DME) injection time significantly influence the combustion and emissions characteristics of the biogas–DME dual fuel in a modified single-cylinder diesel engine. Increasing the biogas to DME mixing ratio reduced the maximum combustion pressure, led to a slower ignition time, and decreased the increasing combustion pressure. As the biogas mixing ratio increased, the peak and gradient of heat release rate (ROHR) decreased [63]. Increasing the oxygen concentration to 27% in the air supplied to the dual fuel results in lower fuel ignition times and methane emissions. At 40 brake thermal efficiency (BTE) engine load increased to 28% [64]. The use of diethyl ether (DEE) in dual-fuel biogas engines shows that the biogas–DEE HCCI mode shows a higher operating load range and higher brake thermal efficiency (BTE) at full load compared to biodiesel and biogas SI (spark ignition) modes [65]. In the bi-fuel mode, the biogas/biodiesel blend engine achieved maximum pressure compared to the biogas/diesel low-load engine, but slightly lower heat output. At 60% load, biogas and biodiesel combustion showed slightly higher pressures, heat dissipation rates (ROHR), and average effective pressures (IMEP) than biogas diesel engines [66].

A cheap source of biodiesel finding is a very pressing issue in today's fuel production [67–70]. Thus, the alcohols will be used in the processing of forest, food, and other biomass waste if it is suitable for use as a fuel in the transport sector. One of these products is HVO (Hydrogenated Vegetable Oil), which has huge resources [71]. Policies and regulations have a direct impact on the use and production of HVO on a global scale [72]. It is renewable and has properties similar to diesel [73]. Its use improves the environmental performance of the engine: significant reduction in CO and HC emissions and a slight positive impact on NO_x, CO₂, and smoke/PM emissions and engine power [74]. This tendency is also noticeable when operating vehicles fuelled by HVO mixtures and under adverse environmental conditions (up to –7 °C) [75]. In addition, no significant difference in spray dynamics between HVO and EN590 was observed, which also promotes the use of such fuels [76]. Table 1 lays down the properties of the analyzed fuel [53,56,77–80].

The aim of the research was to find the change in energy and environmental parameters of a compression ignition engine having used the dual fuel power system and with the engine running on different fuels: diesel–natural gas, diesel–biogas, HVO–natural gas, and HVO–biogas and when changing SOI. This study is relevant because there are few studies by other authors that use 100% biofuels in dual-fuel engines: biodiesel (HVO) and biogas (biomethane).

Table 1. Main characteristics of the fuels.

Properties	Diesel	HVO	Natural Gas	Biogas
Lower heating value <i>LHV</i> , MJ/kg	42.5	44.1	50.0	19.1
Cetane number	52.1	>70.0	-	-
Octane number	-	-	>120	130
Auto-ignition temperature, °C	180–220	-	650	600–650
Stoichiometric air-fuel ratio, kg/kg	14.3	-	17.2	6.17
Carbon content, %	87	84.36	75	-
Flammability limits, vol. % in air	0.6–7.5	-	5–15	7.5–14

HVO—Hydrogenated Vegetable Oil.

2. Materials and Methods

Experimental research of energy and environmental indicators of a compression ignition engine running on diesel and gas (dual fuel) was conducted using the 1.9 TDI (Turbocharged Direct Injection) (1Z) engine loaded using the engine load bench. The CI engine power system comprises the electronically controlled axial-piston distributor injection pump BOSCH VP37 and a hole-type two-springs nozzle (opening pressure 190–200 bar). The engine was equipped with a turbocharger and a wastegate as a boost-controlling device. Table 2 presents the key indicators of the CI 1.9 TDI engine, also using the additional gas supply system Dual fuel (Elpigaz-Degamix) for supplying natural gas (NG). CO₂ was supplied separately controlling its amount using a pressure reducer. NG and CO₂ gas were supplied to the intake manifold ahead of the turbocharger (Figure 1).

Table 2. Key parameters of the 1.9 TDI (1Z) compression ignition engine.

Parameter	Value
Engine capacity V_H , cm ³	1986
Number of cylinders	4
Gas distribution system	OHC
Degree of compression,	19.5
Piston diameter D , mm	79.5
Piston stroke S , mm	95.5
Power P , kW	66 (4000 rpm)
Torque M , Nm	182 (2000–2500 rpm)
Pressure of the opening of the fuel injector p_i , bar	190

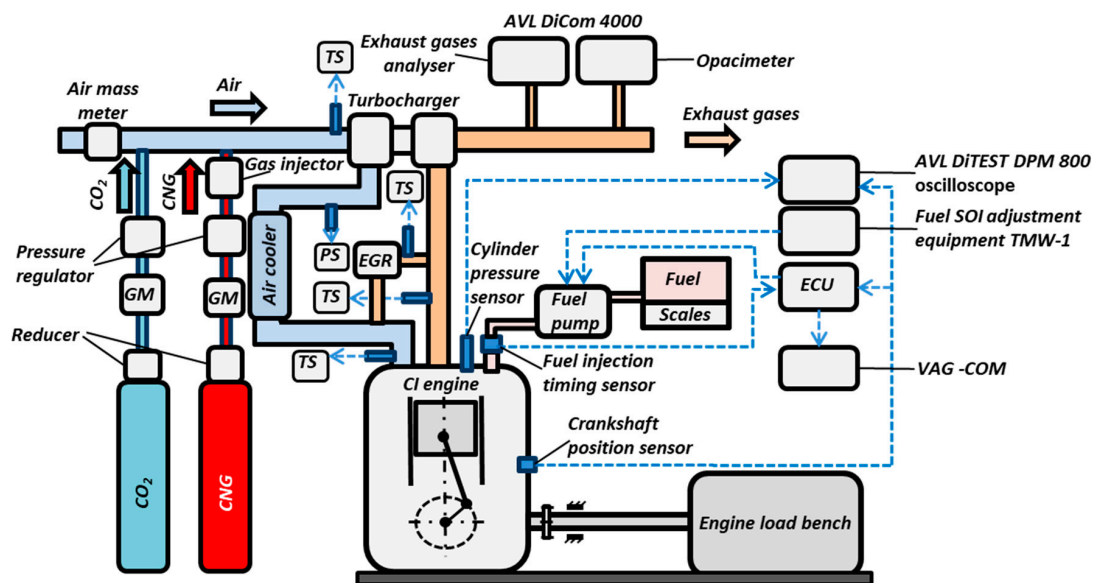


Figure 1. Engine test equipment.

The load bench KI-5543 was used to determine the engine's brake torque M_B (Nm) and the shaft speed n (rpm). M_B measurement error = ± 1.23 Nm. Electronic scale SK-5000 and a stopwatch was used to determine hourly consumption of diesel B_f (kg/h). Measurement error of fuel consumption—0.5%. Consumption of NG and CO₂ was measured using the gas mass flow meter Type RHM 015 with the accuracy of $\pm 0.1\%$. The intake air mass was measured using the meter BOSCH HFM 5 with the accuracy of 2%. VAG-Com is communicating via OBD II-ECU and displays SOI information. The pressure in the cylinder was captured using a piezoelectric sensor mounted on a spark plug AVL GH13P with a sensitivity of 15.84 ± 0.09 pC/bar. Photoelectric encoder A58M-F (Precizika Metrology, Žirmūnų st. 139, Vilnius 09120, Lithuania) with a signal repeatability of 0.35156 CAD was used to determine the position of the crankshaft. The value of the gas pressure in the cylinder was recorded using the AVL DiTEST DPM 800 oscilloscope (input range 6000 pC, signal ratio 1 mV/pC) and the LabView Real software. 100 cycles in the pressure cylinder were measured, also calculating the average pressure values at each measuring point. The pressure was measured in the engine intake manifold using the pressure sensor (PS) Delta OHM HD 2304.0 m with a measurement error of ± 0.0002 MPa. The temperature was measured using type K thermocouples Temperature sensors (TS) the accuracy of ± 1.5 °C. Engine's exhaust gas composition was determined using the exhaust gas analyzer and the opacimeter AVL DiCom 4000. Its parameters are listed in Table 3. During the experiment, constant ambient parameters were maintained: intake air temperature—17 °C, air pressure—1000.6 hPa, relative humidity—52%. The number of experiments for repetitions was five, averaging the results.

Table 3. Measurement range and accuracy of the exhaust gas analyzer.

Parameter	Measurement Range	Accuracy
CO	0–10 vol. %	0.01 vol. %
CO ₂	0–20 vol. %	0.1 vol. %
HC	0–20,000 ppm vol.	1 ppm
NO _x	0–5000 ppm vol.	1 ppm
O ₂	0–25 vol. %	0.01 vol. %
λ	0–9.999	0.001
Smoke absorption coefficient	0–99.99 m ⁻¹	0.01 m ⁻¹
Engine speed	250–9990 rpm	10 rpm

During the test, the engine speed was $n = 2000$ rpm and the engine brake torque— $M_B = 45$ Nm. These are the operating conditions of the engine in urban conditions. Tests were performed with a disconnected EGR valve, because excess air ratio decreases significantly when using biogas containing 40% of CO₂.

Liquid fuels and dual fuels were used in the experimental research. Conventional diesel fuel (D) and the second generation biodiesel hydrotreated vegetable oil (HVO) were used as liquid fuels. The gaseous fuels used were also of two types: natural gas and biogas. Methane comprises the major part of the natural gas energy. It is marked as BM. The composition of biogas was simulated supplying CO₂ gas together with NG (CO₂ comprised 40% of NG volume). Table 4 presents the composition of the fuel used in the research (by energy of individual components), the marking of fuel in graphs and the lower heating value (LHV). The lower heating value of fuel mixtures was calculated by determining the LHV of the individual components and their mass concentration.

Table 4. Fuels used during the test and their marking.

Fuel Composition		Marking	LHV, MJ/kg
Liquid Fuel (% of Energy)	Gaseous Fuel (% of Energy)		
Conventional diesel fuel (100%)	-	D100	42.80
Conventional diesel fuel (40%)	Natural gas methane (60%)	D40/M60	46.55
Conventional diesel fuel (40%)	Natural gas methane (60%) + CO ₂	D40/BM60	22.73
Hydrotreated Vegetable Oil (100%)	-	HVO100	43.65
Hydrotreated Vegetable Oil (40%)	Natural gas methane (60%)	HVO40/M60	46.90
Hydrotreated Vegetable Oil (40%)	Natural gas methane (60%) + CO ₂	HVO40/BM60	22.88

Numerical simulation of the analyzed operation of the engine was done using the AVL BOOST software in application of the approved methodologies for physical processes that take place in the engine. To create the model of an internal combustion engine, general engine parameters were entered into the AVL BOOST software, such as the cylinder diameter, stroke, compression ratio, crank length, shaft revolutions, number of engine strokes, cylinder operating order, valve phases and opening stroke, amount of remaining fuel in the cylinder, and friction in the engine at different engine speeds. Engine parameters such as intake and exhaust tract lengths, diameters, pipe lengths, diameters, angles and other were measured in real engine. Intake and exhaust volume, a turbocharger and other parameters were determined. Figure 2 presents a graphical image of the numerical model of the engine.

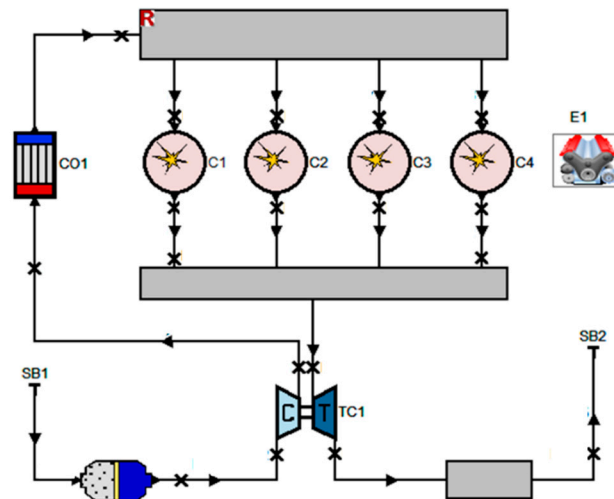


Figure 2. Development of a digital model of the engine.

The Vibe function was used to determine the heat dissipation characteristics of the engine [81]:

$$ROHR = \frac{dx}{d\varphi} = \frac{6.908}{\varphi_{CD}} \cdot (m_v + 1) \cdot \left(\frac{\varphi - \varphi_{SOC}}{\varphi_{CD}} \right)^{m_v} \cdot e^{-6.908 \cdot \left(\frac{\varphi - \varphi_{SOC}}{\varphi_{CD}} \right)^{(m_v+1)}}, \quad (1)$$

$$dx = \frac{dQ}{Q}, \quad (2)$$

where Q —total fuel heat input; φ —crank angle; m_v —combustion shape parameter; φ_{SOC} —start of combustion; $\Delta\varphi_{CD}$ —combustion duration.

The share of the fuel mass which was burnt since the start of the combustion process was determined by integrating the Vibe function:

$$MFB = \int \frac{dx}{d\varphi} \cdot d\varphi = 1 - e^{-6.908 \cdot \left(\frac{\varphi - \varphi_{SOC}}{\varphi_{CD}} \right)^{(m_v+1)}}. \quad (3)$$

The main combustion parameters, including MFB , $ROHR$, φ_{SOC} , $\Delta\varphi_{CD}$, m_v , and others, were determined using the BURN sub-software of the AVL BOOST software and the parameters measured during the experiment (the pressure of the operating cycle in the cylinder p ; the cyclic mass of the injected fuel m_{c_f} , the cyclic air mass m_{c_air} , fuel LHV, and others).

3. Research Results and Discussion

With the compression ignition engine 1.9 TDI (1Z) running of pure diesel or biodiesel ($n = 2000$ rpm, engine brake torque, $M_B = 45$ Nm), the engine control unit (ECU) software algorithm plans for SOI of about 6 CAD BTDC. Such SOI value was determined taking into account environmental and energy parameters of the engine (Figures 3–10). With the engine running on dual fuel (liquid and gaseous),

where the energy from liquid fuel accounts for 40% and from gaseous fuel for 60%, the engine's ECU provides for SOI of liquid fuel of about 1.5 CAD BTDC. When using dual fuel, liquid fuels are injected later as their amount decreases, and the injection and burning of liquid fuels requires less time. Having replaced diesel with dual fuel in a compression ignition engine, the fuel combustion process also changes, so determining the energetic and environmental parameters over a wide SOI range would be expedient. The results obtained were compared with diesel indicators.

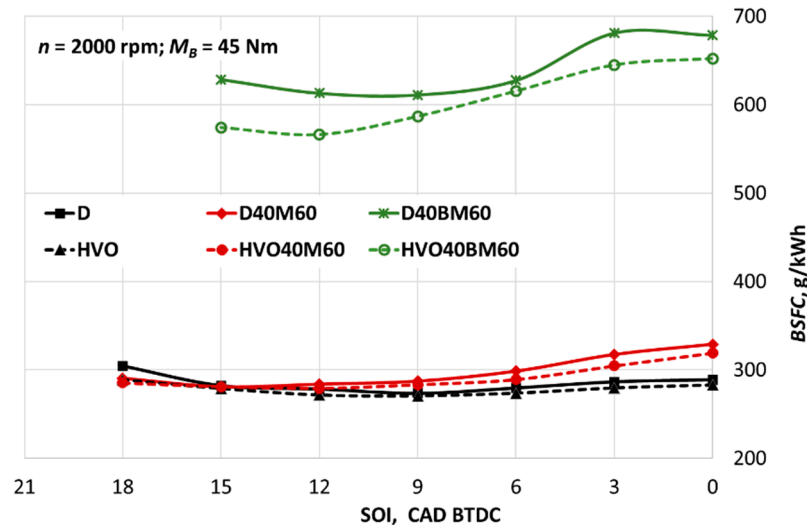


Figure 3. Change of the brake specific fuel consumption depending on fuel composition and start of injection (SOI).

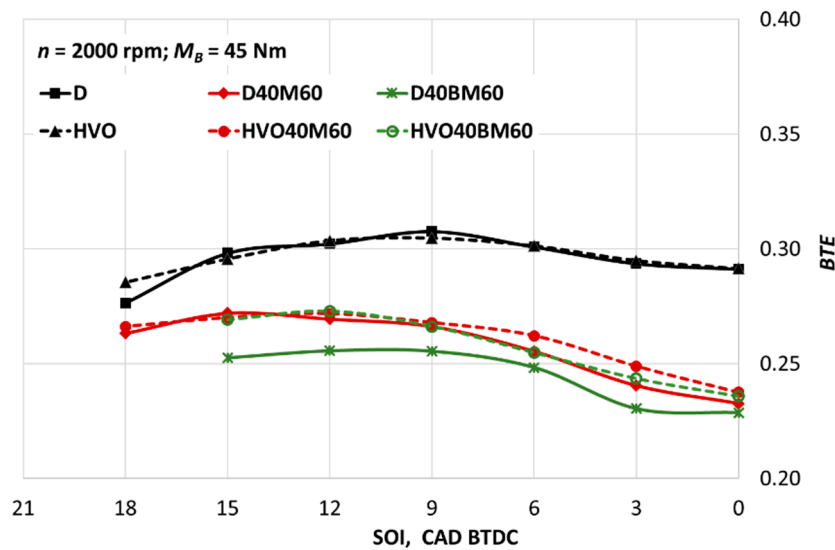


Figure 4. Change of the Brake Thermal Efficiency depending on fuel composition and SOI.

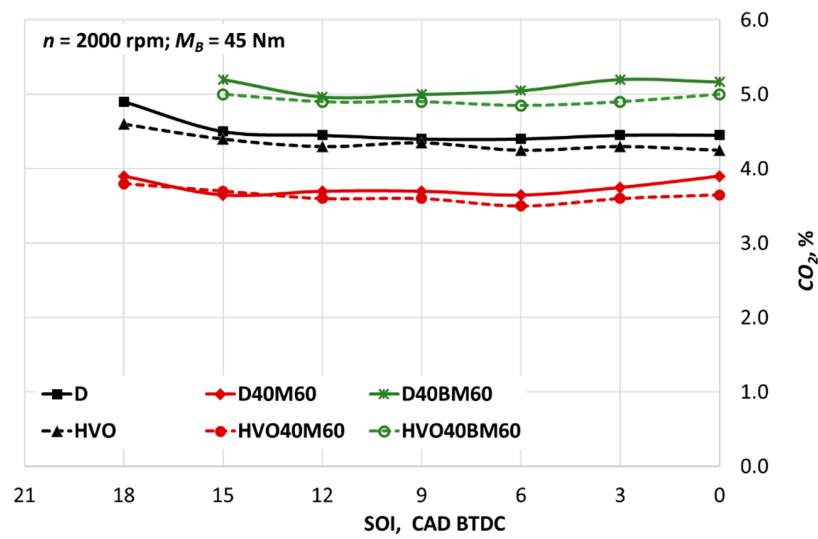


Figure 5. Change of CO₂ volumetric fraction depending on fuel composition and SOI.

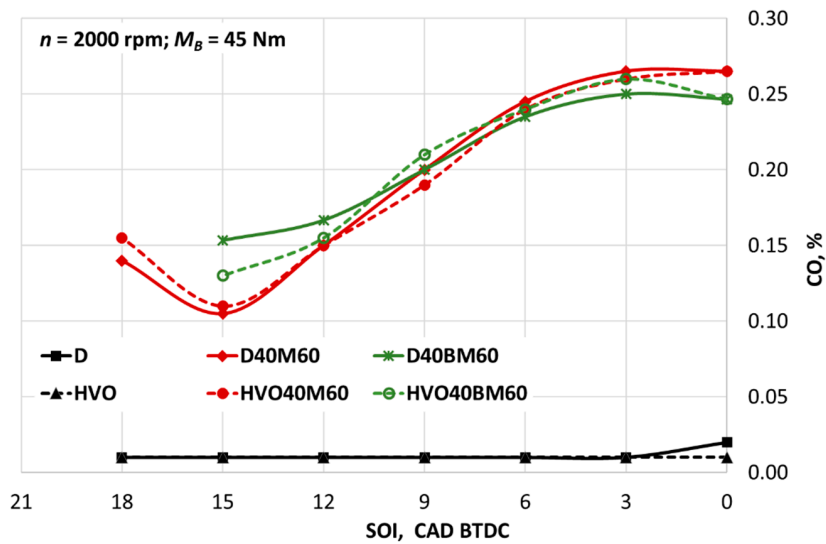


Figure 6. Change of CO volumetric fraction depending on fuel composition and SOI.

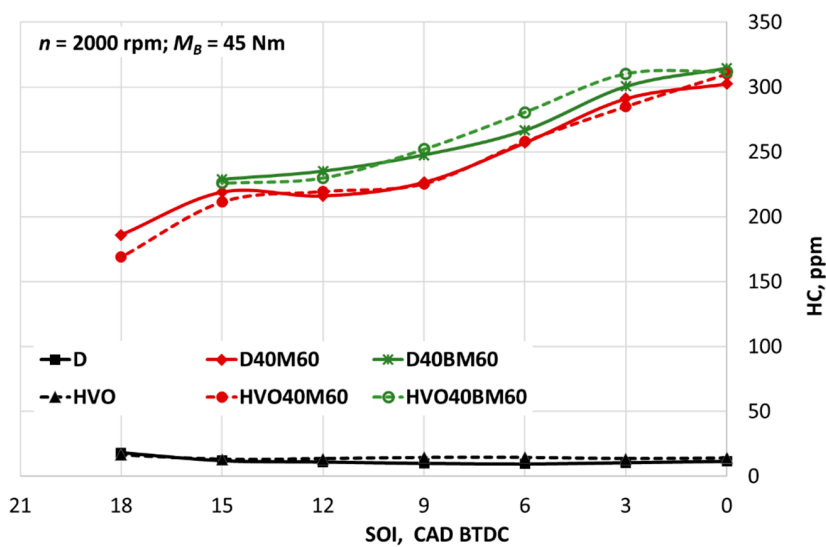


Figure 7. Change of HC volumetric fraction depending on fuel composition and SOI.

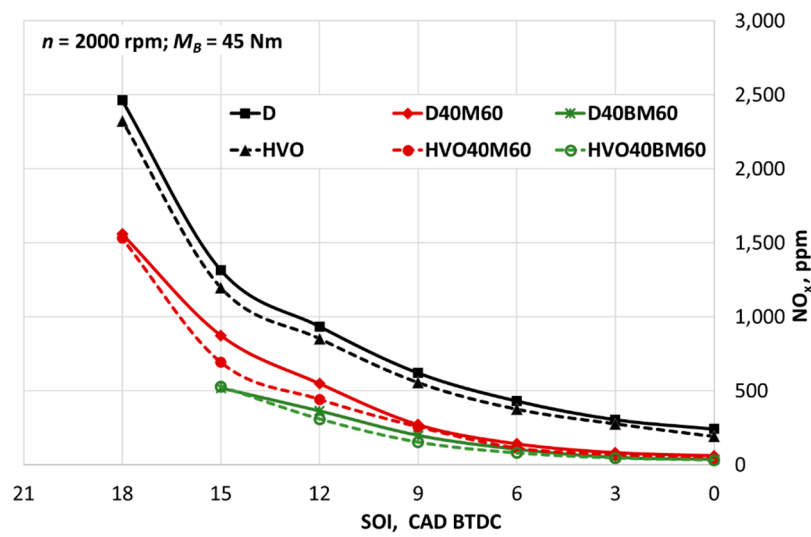


Figure 8. Change of NO_x volumetric fraction depending on fuel composition and SOI.

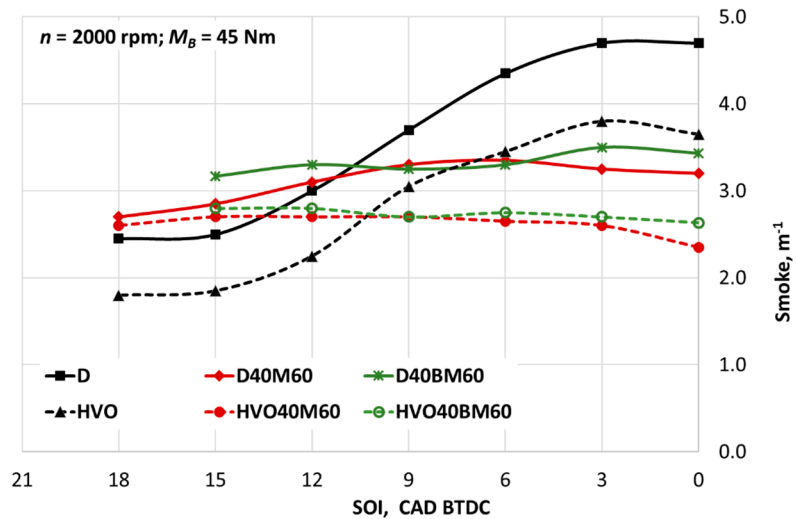


Figure 9. Change of smoke depending on fuel composition and SOI.

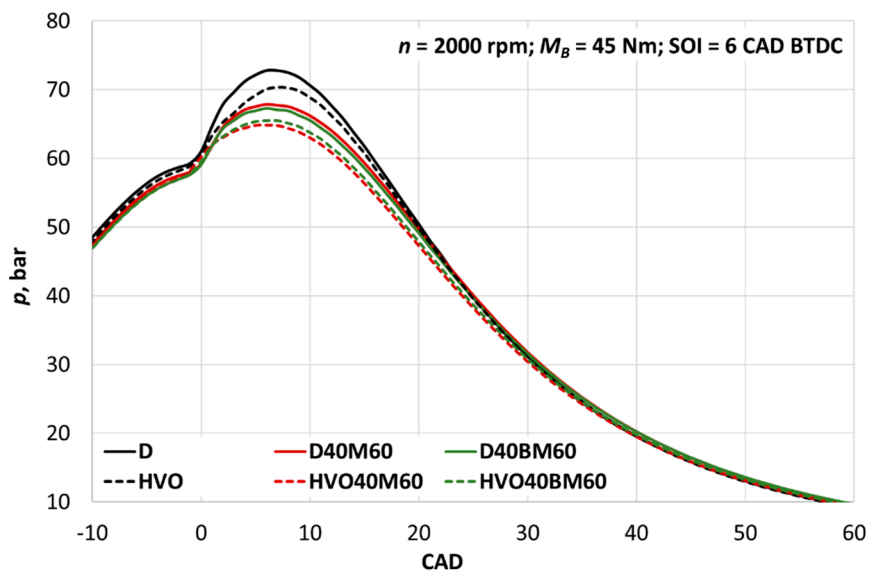


Figure 10. Pressure in the cylinder depending on fuel composition.

3.1. Energy Indicators

The lowest Brake Specific Fuel Consumption (BSFC) was achieved throughout the entire range of SOI research (0–18 CAD BTDC) with the engine running on HVO fuel with a high (43.65 MJ/kg) LHV. With SOI being 6 CAD BTDC, consumption of HVO fuel was 2.1% lower compared to diesel fuel, because HVO's LHV is 2.0% higher. The additional supply of methane increased BSFC: D40M60—6.8%, HVO40M60—3.3%, even though the LHV of D40M60 was 8.8% higher and LHV of HVO40M60 was 9.6% higher (Figure 3). The changed combustion process resulted in a higher fuel consumption. Compared to diesel fuel, additional supply of biomethane significantly increased the BSFC: D40BM60 by 124.5% and HVO40BM60 by 120.1%. Using biomethane, the fuel mass consumption increased, because LHV of D40BM60 was 46.9% lower than that of diesel and LHV of HVO40BM60 was 46.6% lower. Dual fuel BSFC declined advancing SOI to 12–15 CAD BTDC, because of a more complete gas combustion, which is evident from a declined volumetric fraction of incomplete combustion products (CO, HC, and Smoke) in exhaust gases (Figures 6, 7 and 9).

With the engine running on diesel and HVO fuel, the values of the Brake Thermal Efficiency (BTE) are close in the entire SOI range. Compared to diesel, with the engine running on dual fuel with added methane, BTE decreased: D40M60 by 14.1% and HVO40M60 by 11.9%. The use of a biomethane additive reduced BTE: D40BM60 by 16.5% and HVO40BM60 by 14.3%. HVO partially offset the reduction in BTE, especially when using dual fuel with biomethane gas.

3.2. Environmental Indicators

When using dual fuel comprising methane, CO₂ concentration declined compared to conventional diesel fuel, with SOI being 6 CAD BTDC: D40M60 by 17.1% and HVO40M60 by 20.4% (Figure 5). This was due to a lower methane C/H ratio. When using biogas, CO₂ volumetric fraction increased (D40BM60 by 14.8% and HVO40BM60 by 10.2%), because CO₂, which does not take part in combustion, comprised 40% of the biomethane gas. However, biomethane is a renewable fuel, and taking into account its complete life cycle, this increase in CO₂ emissions is insignificant. Having replaced conventional diesel fuel with renewable HVO reduces CO₂ concentration by 3.4% as HVO has a lower C/H ratio. When advancing the injection moment from SOI 0 CAD to 6–12 CAD BTDC, CO₂ volumetric fraction decreases due to increasing engine efficiency and decreasing fuel consumption.

A change in the volumetric fraction of HC and carbon monoxide in unburned hydrocarbons is clearly correlated with engine running on fuel of different composition and changing SOI (Figures 6 and 7). With the engine running on all tested dual fuels and the SOI being 6 CAD BTDC, the CO volumetric fraction increased from 0.01% to ~0.24% (~24 times) compared to conventional diesel fuel (Figure 6), while HC volumetric fraction increased from 9.5 ppm to 257–280 ppm (~28 times) (Figure 7). The combustion process deteriorates because of lean gas concentration in the air (air–gas fuel ratio ~7), when gas does not burn sufficiently. The comparison of methane and biomethane as dual fuel revealed that CO and HC emissions changed slightly, even though biogas contains 40% CO₂, which suppresses combustion. However, in the event of excessive air excess, CO₂ gas has little effect on combustion. The HC volumetric fraction also increases due to the fact that injection and exhaust valves, which are used to blow methane gas to the exhaust manifold, overlap at the end of the exhaust stroke and at the start of the intake stroke. Using dual fuel and having advanced the SOI timing to 12–15 CAD BTDC, CO volumetric fraction decreased to 0.10–0.15% and HC volumetric fraction decreased to 210–230 ppm as the combustion temperature increased and the combustion process improved.

When using dual fuel, which contains methane, NO_x volumetric fraction compared to conventional diesel fuel, when SOI is 6 CAD BTDC, decreased: D40M60 –by 67% and HVO40M60 by 74% (Figure 5). When using biomethane gas, NO_x volumetric fraction decreased even more (D40BM60 by 76% and HVO40BM60 by 82%). Dual fuel reduced the amount of liquid fuels, which in turn reduced the combustion intensity and heat release in the kinetic (premixed) combustion phase. An even more intense heat release occurs in the diffusion phase with gaseous fuel combustion. The CO₂ gas in

biomethane additionally suppresses the combustion process. HVO fuels also reduce NO_x volumetric fraction (6–12%) as these biofuels have a higher cetane number and, thus, shorten the ignition delay phase, while heat release declines in the premixed phase. By advancing SOI timing, the NO_x volumetric fraction in the exhaust gas increases significantly operating on all tested fuel blends, because combustion occurs at a lower volume and higher temperatures.

When using dual fuel, ensuring the SOI timing 6 CAD BTDC provided for by the engine control unit (ECU) software algorithm and having replaced conventional diesel with HVO fuels, smoke decreased by 23% (Figure 9). This comes as a result of a lower C/H ratio of HVO fuels and the combustion process: ROHR of HVO is more intense at the diffusion phase, which allows for a better combustion of soot. The use of dual fuel containing methane allowed reducing smoke compared to pure conventional diesel: D40M60 by 23% and HVO40M60 by 39% (Figure 5). The use of dual fuel containing biomethane allowed reducing smoke: D40M60 by 24% and HVO40M60 by 37%. The reduction of smoke achieved using methane and biomethane gases was almost the same, because both gases contain methane, which accounts for 60% of fuel energy. Methane has a simple molecular structure and is completely combustible. Gaseous fuels increased the combustion intensity during the diffusion phase and helped to burn the soot formed during the combustion of liquid fuels.

Advancing the SOI timing to 12–15 CAD BTDC, the HVO fuel smoke level significantly decreased, because combustion takes place at higher temperatures. However, the smoke of dual fuel remained nearly the same when advancing SOI timing, and when using biomethane gas, a slight increase in the smoke level was observed.

There were calculated excess air ratio (SOI timing 6 °CAD BTDC) for diesel (D) 3.3, D40M60 2.8, D40BM60 2.7, HVO 3.4, HVO40M60 2.9, D40BM60 2.8. Replacing diesel with HVO fuel reduced the air excess value due to the lower C/H ratio. Methane has reduced the air excess value by occupying volume and reducing the air mass in the cylinder. CO_2 and air are in excess value in biomethane. However, the reduced air excess value for M and BM gas did not increase the smoke due to the specific composition of the gas.

The pollutant emissions of the engine are estimated by measuring the volumetric fraction of the pollutants in the exhaust gas. The estimation of the pollutant volumetric fraction is objective if the volumetric flow of the flue gas is the same for all fuels tested. The engine operating mode was constant during the study ($M_B = 45 \text{ Nm}$ and $n = 2000 \text{ rpm}$). In dual fuel mode, the air mass consumption is reduced by up to 2%, as part of the volume is occupied by methane or biomethane and the volumetric flow of flue gas is minimized.

3.3. Combustion Indicators

When using the BURN sub-software of AVL BOOST software, the use of the parameters measured during the experiment (operating cycle pressure in the cylinder p (Figure 10) and others) allowed for the determination of key combustion parameters (Figures 11–13). With the engine operating in the mode $n = 2000 \text{ rpm}$, brake torque $M_B = 45 \text{ Nm}$ and SOI = 6 CAD BTDC, the maximum combustion pressure in the cylinder (72.8 bar) is reached using conventional diesel (Figure 10). The maximum combustion pressure of HVO fuels decreased by 3.3%, D40M60 by 6.8%, HVO40M60 by 10.9%, D40BM60 by 7.6%, and HVO40BM60 by 10.1%. All of the fuels reached the maximum pressure at 6–7 CAD ATDC.

The maximum rate of heat release (37.2 J/CAD at 1 CAD ATDC) was achieved using conventional diesel (Figure 11). The maximum ROHR of HVO fuel decreased by 31% at 1 CAD ATDC, D40M60 17% at 1 CAD ATDC, HVO40M60 49% at 8 CAD ATDC, D40BM60 19% at 1 CAD ATDC, and HVO40BM60 48% at 8 CAD ATDC. Reduced heat release in the kinetic (premixed) combustion phase decreased the temperature and the intensity of NO_x formation. The combustion of HVO fuels can be characterized by a more intense fuel release in the diffusion phase. Methane gases contained in dual fuel burn at a lower intensity and significantly increase the ROHR in the diffusion phase, which in turn improves the combustion of soot. This is confirmed by the parameter describing the intensity (combustion shape parameter m_v) (Table 4).

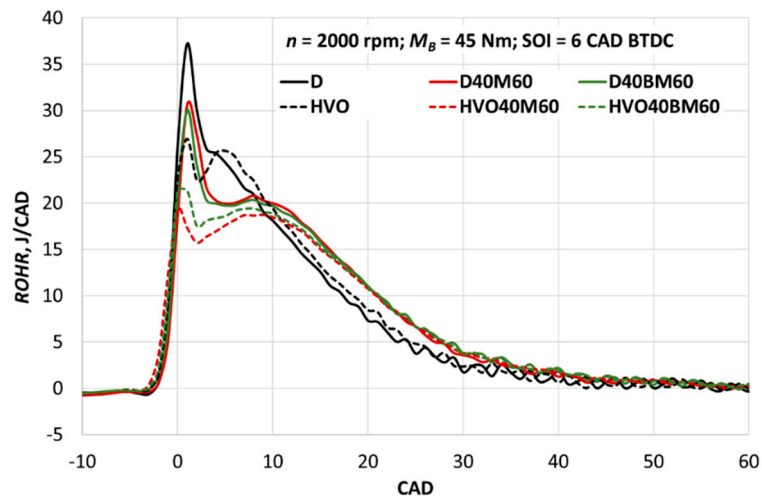


Figure 11. Rate of heat release in the cylinder depending on fuel composition.

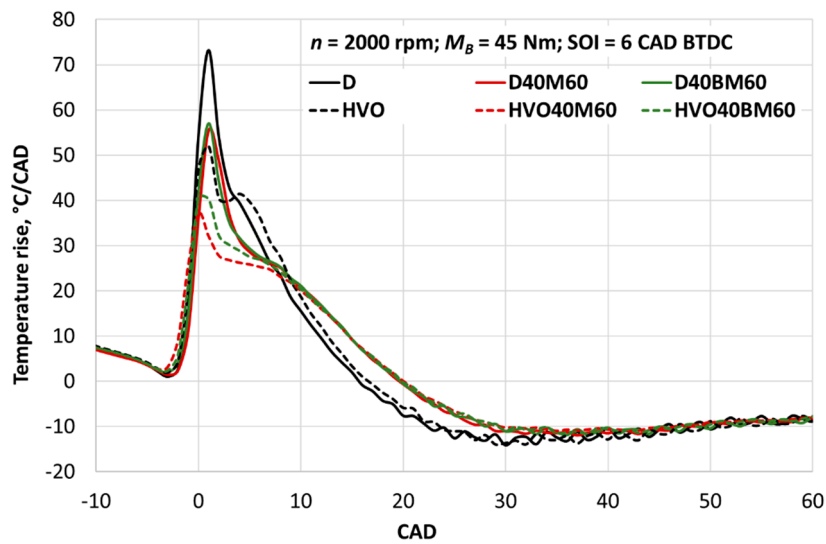


Figure 12. Temperature rise in the cylinder depending on fuel composition.

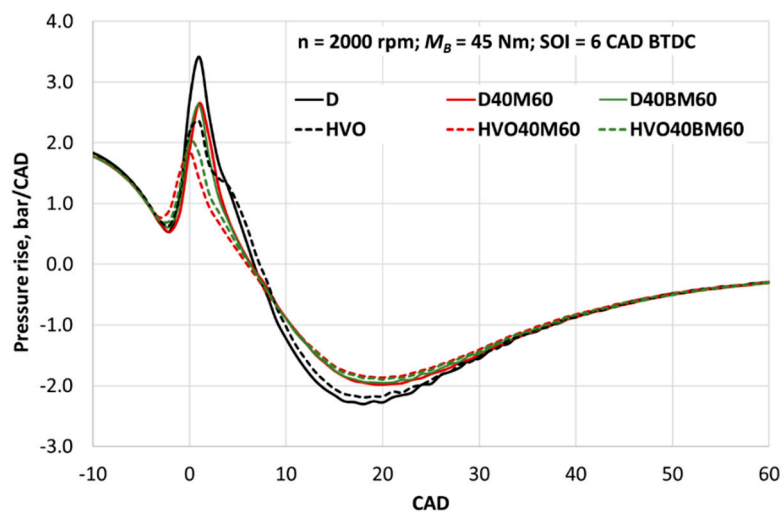


Figure 13. Pressure rise in the cylinder depending on fuel composition.

The maximum temperature rise for all types of fuel was reached at 1 CAD ATDC. The values of the temperature rise indicator correlate with ROHR. The maximum value was reached (73 °C/CAD) using conventional diesel (Figure 12). The maximum temperature rise of HVO declined by 29%, D40M60 by 24%, HVO40M60 by 56%, D40BM60 by 22%, and HVO40BM60 by 45%. However, HVO fuels create a higher temperature rise in the diffusion phase, while when using dual fuel, this effect of a longer combustion process is even more obvious.

The maximum pressure rise (3.4 bar/CAD) was reached using conventional diesel (Figure 13). The maximum pressure rise of HVO fuels decreased by 31%, D40M60 by 22%, HVO40M60 by 46%, D40BM60 by 23%, and HVO40BM60 by 41%.

The maximum pressure rise for all fuels was reached at TDC or 1 CAD ATDC. The value of the maximum pressure rise was also significantly affected by the replacement of conventional diesel with HVO biofuels and the use of dual fuel. Having reduced the maximum pressure rise, the load on engine parts and engine noise decreased.

ROHR schedule (Figure 11) shows that the SOC (Start Of Combustion) timing (φ_{SOC}) of all the analysed fuels differs very slightly and is 2–3 CAD BTDC. Combustion ($\Delta\varphi_{CD}$) is the shortest using conventional diesel (50.7 CAD). When using HVO fuel, combustion duration increased by 1.8%, D40M60 by 4.5%, HVO40M60 by 7.7%, D40BM60 by 10.1%, and HVO40BM60 by 9.9% (Table 5).

Table 5. Combustion indicators of fuel mixtures.

Combustion Indicators	Fuel					
	D100	D40/M60	D40/BM60	HVO100	HVO40/M60	HVO40/BM60
Combustion duration $\Delta\varphi_{CD}$, CAD	50.7	53	55.8	51.6	54.6	55.7
Combustion shape parameter m_v	0.684	1.08	1.06	0.848	1.11	1.09

The ROHR and the combustion shape parameter (m_v) determined by numerical modelling revealed that having replaced conventional diesel fuel with HVO fuels, the maximum heat release shifts towards the end of combustion. The analysis of all the analyzed dual fuels (D40M60, HVO40M60, D40BM60, and HVO40BM60) ROHR and the combustion shape parameters determine that gas combustion is slower, and a significant share of heat is released closer to the end of combustion.

4. Conclusions

Having conducted the experimental and numerical modelling research of a CI engine ($V_H = 1986 \text{ cm}^3$, $n = 2000 \text{ rpm}$, $M_B = 45 \text{ Nm}$, and $\text{SOI} = 6 \text{ CAD BTDC}$) and after replacing conventional diesel (D) with a dual fuel (D, HVO–M, or BM) where gas energy amounts for 60% of fuel mixture, the following conclusions can be made:

1. When using dual fuel D40M60, BSFC increased by 6.8% and BTE decreased by 14.1%, while when using HVO40BM60, BSFC grew 1.2 times and BTE decreased by 14.3%. The use of biomethane gas significantly increased fuel consumption, because CO_2 comprised 40% of BM gas volume, while LHV of biogas was ~2.7 times lower than that of methane. The use of both methane and biomethane gas reduced BTE because of the changed combustion process.
2. With the engine running on D40M60, CO_2 emissions declined by 17.1%, because methane has a lower C/H ratio. When using HVO40BM60, CO_2 emissions increased by 10.2%, even though the C/H ratio of HVO biodiesel and methane was lower compared to that of the conventional diesel fuel. CO_2 emission was increased due to the fact that CO_2 comprised 40% of BM volume. However, biomethane is a renewable fuel and produces lower CO_2 emissions throughout its life cycle.
3. CO volumetric fraction of dual fuel (D40M60 and HVO40BM60) increased from 0.01% to ~0.24% (~24 times), while HC volumetric fraction grew from 9.5 ppm to 257–280 ppm (~28 times). Emissions of incomplete combustion products increased due to the reduction of excess air ratio

and lower combustion temperatures. HC emissions also increased due to the overlap of intake and exhaust valves.

4. With the engine running on D40M60, NO_x emission decreased by 67%, and when using HVO40BM60, it decreased by 82%. The use of dual fuel reduced the amount of liquid fuels, which create an intense combustion and heat release in the kinetic (premixed) combustion phase. Cetane number is higher in HVO fuels, which reduces the ignition delay phase and ROHR. CO₂ gases contained in biomethane also suppress ROHR.
5. The use of dual fuel D40M60 reduced smoke by 23%, and using HVO40BM60, smoke declined by 39%. HVO fuels have a lower C/H ratio and a more intensive combustion in the diffusion phase. Methane has a simpler molecular structure, a lower C/H ratio and a longer combustion time. All this helped to burn soot having formed in the course of the combustion of liquid fuels.
6. A lower ROHR in the premixed combustion phase (D40M60 and HVO40BM60) decreased a temperature rise and NO_x formation. A lower pressure rise results in a lesser load on the engine's crankshaft mechanism parts, and the engine produces less noise. When using HVO biogases, ROHR is more intense in the diffusion phase, methane and CO₂ gases also affect a delayed heat release and a longer combustion process, which in turn reduces smoke, also reducing BTE. In pursuit of the maximum BTE for dual fuels, SOI must be advanced. This will reduce CO and HC emissions, leaving smoke levels nearly the same, but significantly increasing NO_x emissions.

Author Contributions: Conceptualization, A.R. and S.S.; methodology, A.R., S.S., and J.M.; software, S.S. and A.R.; formal analysis, A.R. and J.M.; validation, A.R. and S.S.; writing—original draft preparation, A.R. and J.M.; writing—review and editing, A.R. and J.M.; supervision, A.R., and J.M.; project administration, J.M. All authors have read and agreed to the published version of the manuscript.

Funding: This research received no external funding.

Acknowledgments: Authors are grateful to JSC “NESTE Lietuva” for providing the possibility to test the advanced hydrotreated vegetable oil called “HVO”. A part of the results of the research described in this article were obtained using the engine simulation tool AVL BOOST, acquired by signing a Cooperation Agreement between AVL Advanced Simulation Technologies and the faculty of the Transport Engineering of Vilnius Gediminas Technical University.

Conflicts of Interest: The authors declare no conflict of interest.

Nomenclature

B_f	hourly fuel consumption (kg/h)
BMEP	Brake Mean Effective Pressure (bar)
BSFC	Brake Specific Fuel Consumption (g/kWh)
BTE	Brake Thermal Efficiency
D	bore (mm)
LHV	Lower heating value (MJ/kg)
M	engine torque (Nm)
M_B	brake torque (Nm)
MBF	Mass Burn Fraction
m_{c_air}	cyclic mass of air (mg/c)
m_{c_f}	cyclic mass of fuel (mg/c)
m_v	combustion shape parameter
P	engine power (kW)
p_i	fuel injector opening pressure (bar)
Q	total fuel heat input (J)
ROHR	Rate of Heat Release (J/CAD)
S	stroke (mm)
V_H	engine displacement (cm ³)
λ	air–fuel equivalence ratio
n	Rotational speed of the crankshaft (rpm)
φ	crank angle (CAD)
φ_{CD}	combustion duration (CAD)
φ_{SOC}	start of combustion (CAD)

Abbreviations

ATDC	After Top Dead Centre
BM	biomethane
BTDC	Before Top Dead Centre
CAD	Crank Angle Degree
HC	hydrocarbons
CH ₄	methane
CI	Compression Ignition
CO	carbon monoxide
CO1	intercooler
C14	cylinders
CO ₂	carbon dioxide
D	diesel fuel
ECU	Engine Control Unit
EGR	Exhaust Gas Recirculation
E1	engine
GM	Gas meter
HVO	Hydrotreated Vegetable Oil
M	methane
NG	Natural Gas
NO _x	nitrogen oxides
O ₂	oxygen
OHC	Overhead Camshaft
PM	Particulate Matter
PS	pressure sensor
SOI	Start of Injection
TC	turbocharger
TDI	Turbocharged Direct Injection
TS	Temperature sensor

References

1. Achinas, S.; Willem Euverink, G.J. Rambling facets of manure-based biogas production in Europe: A briefing. *Renew. Sustain. Energy Rev.* **2019**, *109*, 566. [[CrossRef](#)]
2. Lyng, K.-A.; Stensgård, A.E.; Hanssen, O.J.; Modahl, I.S. Relation between greenhouse gas emissions and economic profit for different configurations of biogas value chains: A case study on different levels of sector integration. *J. Clean. Prod.* **2018**, *182*, 737–745. [[CrossRef](#)]
3. Stürmer, B. Biogas—Part of Austria’s future energy supply or political experiment? *Renew. Sustain. Energy Rev.* **2017**, *79*, 525–532. [[CrossRef](#)]
4. Xue, S.; Song, J.; Wang, X.; Shang, Z.; Sheng, C.; Li, C.; Zhu, Y.; Liu, J. A systematic comparison of biogas development and related policies between China and Europe and corresponding insights. *Renew. Sustain. Energy Rev.* **2020**, *117*, 109474. [[CrossRef](#)]
5. Khalil, M.; Berawi, M.A.; Heryanto, R.; Rizalie, A. Waste to energy technology: The potential of sustainable biogas production from animal waste in Indonesia. *Renew. Sustain. Energy Rev.* **2019**, *105*, 323–331. [[CrossRef](#)]
6. Wainaina, S.; Lukitawesa, S.W.; Taherzadeh, M.J. Bioengineering of anaerobic digestion for volatile fatty acids, hydrogen or methane production: A critical review. *Bioengineered* **2019**, *10*, 437–458. [[CrossRef](#)]
7. Nevzorova, T.; Kutcherov, V. Barriers to the wider implementation of biogas as a source of energy: A state-of-the-art review. *Energy Strategy Rev.* **2019**, *26*, 100414. [[CrossRef](#)]
8. Ottosson, M.; Magnusson, T.; Andersson, H. Shaping sustainable markets—A conceptual framework illustrated by the case of biogas in Sweden. *Environ. Innov. Soc. Transit.* **2019**. [[CrossRef](#)]
9. Lönnqvist, T.; Sandberg, T.; Birbuet, J.C.; Olsson, J.; Espinosa, C.; Thorin, E.; Grönkvist, S.; Gómez, M.F. Large-scale biogas generation in Bolivia—A stepwise reconfiguration. *J. Clean. Prod.* **2018**, *180*, 494–504. [[CrossRef](#)]
10. Weinand, J.M.; McKenna, R.; Karner, K.; Braun, L.; Herbes, C. Assessing the potential contribution of excess heat from biogas plants towards decarbonising residential heating. *J. Clean. Prod.* **2019**, *238*, 117756. [[CrossRef](#)]

11. Winquist, E.; Rikkonen, P.; Pyysiäinen, J.; Varho, V. Is biogas an energy or a sustainability product? - Business opportunities in the Finnish biogas branch. *J. Clean. Prod.* **2019**, *233*, 1344–1354. [[CrossRef](#)]
12. Das, S.; Kashyap, D.; Kalita, P.; Kulkarni, V.; Itaya, Y. Clean gaseous fuel application in diesel engine: A sustainable option for rural electrification in India. *Renew. Sustain. Energy Rev.* **2020**, *117*, 109485. [[CrossRef](#)]
13. Cucchiella, F.; D'Adamo, I.; Gastaldi, M. An economic analysis of biogas-biomethane chain from animal residues in Italy. *J. Clean. Prod.* **2019**, *230*, 888–897. [[CrossRef](#)]
14. Bößner, S.; Devisscher, T.; Suljada, T.; Ismail, C.J.; Sari, A.; Mondamina, N.W. Barriers and opportunities to bioenergy transitions: An integrated, multi-level perspective analysis of biogas uptake in Bali. *Biomass Bioenergy* **2019**, *122*, 457–465. [[CrossRef](#)]
15. Pilloni, M.; Hamed, T.A.; Joyce, S. Assessing the success and failure of biogas units in Israel: Social niches, practices, and transitions among Bedouin villages. *Energy Res. Soc. Sci.* **2020**, *61*, 101328. [[CrossRef](#)]
16. Hakawati, R.; Smyth, B.M.; McCullough, G.; De Rosa, F.; Rooney, D. What is the most energy efficient route for biogas utilization: Heat, electricity or transport? *Appl. Energy* **2017**, *206*, 1076–1087. [[CrossRef](#)]
17. Ferella, F.; Cucchiella, F.; D'Adamo, I.; Gallucci, K. A techno-economic assessment of biogas upgrading in a developed market. *J. Clean. Prod.* **2019**, *210*, 945–957. [[CrossRef](#)]
18. Ammenberg, J.; Anderberg, S.; Lönnqvist, T.; Grönkvist, S.; Sandberg, T. Biogas in the transport sector—Actor and policy analysis focusing on the demand side in the Stockholm region. *Resour. Conserv. Recycl.* **2018**, *129*, 70–80. [[CrossRef](#)]
19. Rimkus, A.; Melaika, M.; Matijošius, J. Efficient and Ecological Indicators of CI Engine Fuelled with Different Diesel and LPG Mixtures. *Procedia Eng.* **2017**, *187*, 504–512. [[CrossRef](#)]
20. Bora, B.J.; Saha, U.K. Optimisation of injection timing and compression ratio of a raw biogas powered dual fuel diesel engine. *Appl. Therm. Eng.* **2016**, *92*, 111–121. [[CrossRef](#)]
21. Kukharonak, H.; Ivashko, V.; Pukalskas, S.; Rimkus, A.; Matijošius, J. Operation of a Spark-ignition Engine on Mixtures of Petrol and N-butanol. *Procedia Eng.* **2017**, *187*, 588–598. [[CrossRef](#)]
22. Rimkus, A.; Matijošius, J.; Bogdevičius, M.; Bereczky, A.; Török, Á. An investigation of the efficiency of using O₂ and H₂ (hydroxile gas -HHO) gas additives in a ci engine operating on diesel fuel and biodiesel. *Energy* **2018**, *152*, 640–651. [[CrossRef](#)]
23. Gutarevych, Y.; Shuba, Y.; Matijošius, J.; Karev, S.; Sokolovskij, E.; Rimkus, A. Intensification of the combustion process in a gasoline engine by adding a hydrogen-containing gas. *Int. J. Hydrogen Energy* **2018**, *43*, 16334–16343. [[CrossRef](#)]
24. Swami Nathan, S.; Mallikarjuna, J.M.; Ramesh, A. An experimental study of the biogas—Diesel HCCI mode of engine operation. *Energy Convers. Manag.* **2010**, *51*, 1347–1353. [[CrossRef](#)]
25. Carlucci, A.P.; Ficarella, A.; Laforgia, D.; Strafella, L. Improvement of dual-fuel biodiesel-producer gas engine performance acting on biodiesel injection parameters and strategy. *Fuel* **2017**, *209*, 754–768. [[CrossRef](#)]
26. Chu, S.; Lee, J.; Kang, J.; Lee, Y.; Min, K. High load expansion with low emissions and the pressure rise rate by dual-fuel combustion. *Appl. Therm. Eng.* **2018**, *144*, 437–443. [[CrossRef](#)]
27. Zavadskas, E.K.; Čereška, A.; Matijošius, J.; Rimkus, A.; Bausys, R. Internal Combustion Engine Analysis of Energy Ecological Parameters by Neutrosophic MULTIMOORA and SWARA Methods. *Energies* **2019**, *12*, 1415. [[CrossRef](#)]
28. Juknelevičius, R.; Rimkus, A.; Pukalskas, S.; Matijošius, J. Research of performance and emission indicators of the compression-ignition engine powered by hydrogen—Diesel mixtures. *Int. J. Hydrogen Energy* **2019**, *44*, 10129–10138. [[CrossRef](#)]
29. Rimkus, A.; Žaglinskis, J.; Stravinskas, S.; Rapalis, P.; Matijošius, J.; Bereczky, Á. Research on the Combustion, Energy and Emission Parameters of Various Concentration Blends of Hydrotreated Vegetable Oil Biofuel and Diesel Fuel in a Compression-Ignition Engine. *Energies* **2019**, *12*, 2978. [[CrossRef](#)]
30. Bhowmick, P.; Jeevanantham, A.K.; Ashok, B.; Nanthagopal, K.; Perumal, D.A.; Karthickeyan, V.; Vora, K.C.; Jain, A. Effect of fuel injection strategies and EGR on biodiesel blend in a CRDI engine. *Energy* **2019**, *181*, 1094–1113. [[CrossRef](#)]
31. Liu, J.; Dumitrescu, C.E. Methodology to separate the two burn stages of natural-gas lean premixed-combustion inside a diesel geometry. *Energy Convers. Manag.* **2019**, *195*, 21–31. [[CrossRef](#)]

32. Papagiannakis, R.G.; Krishnan, S.R.; Rakopoulos, D.C.; Srinivasan, K.K.; Rakopoulos, C.D. A combined experimental and theoretical study of diesel fuel injection timing and gaseous fuel/diesel mass ratio effects on the performance and emissions of natural gas-diesel HDDI engine operating at various loads. *Fuel* **2017**, *202*, 675–687. [[CrossRef](#)]
33. Yang, B.; Zeng, K. Effects of natural gas injection timing and split pilot fuel injection strategy on the combustion performance and emissions in a dual-fuel engine fueled with diesel and natural gas. *Energy Convers. Manag.* **2018**, *168*, 162–169. [[CrossRef](#)]
34. Wu, Z.; Han, Z. Micro-GA optimization analysis of the effect of diesel injection strategy on natural gas-diesel dual-fuel combustion. *Fuel* **2020**, *259*, 116288. [[CrossRef](#)]
35. Park, H.; Shim, E.; Bae, C. Expansion of low-load operating range by mixture stratification in a natural gas-diesel dual-fuel premixed charge compression ignition engine. *Energy Convers. Manag.* **2019**, *194*, 186–198. [[CrossRef](#)]
36. Yousefi, A.; Guo, H.; Birouk, M.; Liko, B. On greenhouse gas emissions and thermal efficiency of natural gas/diesel dual-fuel engine at low load conditions: Coupled effect of injector rail pressure and split injection. *Appl. Energy* **2019**, *242*, 216–231. [[CrossRef](#)]
37. Zhang, Y.; Fu, J.; Shu, J.; Xie, M.; Zhou, F.; Liu, J.; Zeng, D. A numerical investigation of the effect of natural gas substitution ratio (NGSR) on the in-cylinder chemical reaction and emissions formation process in natural gas (NG)-diesel dual fuel engine. *J. Taiwan Inst. Chem. Eng.* **2019**, *105*, 85–95. [[CrossRef](#)]
38. Liu, J.; Ma, B.; Zhao, H. Combustion parameters optimization of a diesel/natural gas dual fuel engine using genetic algorithm. *Fuel* **2020**, *260*, 116365. [[CrossRef](#)]
39. Wang, Z.; Du, G.; Wang, D.; Xu, Y.; Shao, M. Combustion process decoupling of a diesel/natural gas dual-fuel engine at low loads. *Fuel* **2018**, *232*, 550–561. [[CrossRef](#)]
40. Zhang, W.; Chang, S.; Wu, W.; Dong, L.; Chen, Z.; Chen, G. A diesel/natural gas dual fuel mechanism constructed to reveal combustion and emission characteristics. *Energy* **2019**, *179*, 59–75. [[CrossRef](#)]
41. Liu, J.; Zhao, H.; Wang, J.; Zhang, N. Optimization of the injection parameters of a diesel/natural gas dual fuel engine with multi-objective evolutionary algorithms. *Appl. Therm. Eng.* **2019**, *150*, 70–79. [[CrossRef](#)]
42. Chen, W.; Pan, J.; Liu, Y.; Fan, B.; Liu, H.; Otchere, P. Numerical investigation of direct injection stratified charge combustion in a natural gas-diesel rotary engine. *Appl. Energy* **2019**, *233–234*, 453–467. [[CrossRef](#)]
43. You, J.; Liu, Z.; Wang, Z.; Wang, D.; Xu, Y. Impact of natural gas injection strategies on combustion and emissions of a dual fuel natural gas engine ignited with diesel at low loads. *Fuel* **2020**, *260*, 116414. [[CrossRef](#)]
44. Luijten, C.C.M.; Kerckhof, E. Jatropa oil and biogas in a dual fuel CI engine for rural electrification. *Energy Convers. Manag.* **2011**, *52*, 1426–1438. [[CrossRef](#)]
45. Anwar, M.; Rasul, M.G.; Ashwath, N. The synergistic effects of oxygenated additives on papaya biodiesel binary and ternary blends. *Fuel* **2019**, *256*, 115980. [[CrossRef](#)]
46. Anwar, M.; Rasul, M.G.; Ashwath, N. The efficacy of multiple-criteria design matrix for biodiesel feedstock selection. *Energy Convers. Manag.* **2019**, *198*, 111790. [[CrossRef](#)]
47. Anwar, M.; Rasul, M.G.; Ashwath, N. Production optimization and quality assessment of papaya (*Carica papaya*) biodiesel with response surface methodology. *Energy Convers. Manag.* **2018**, *156*, 103–112. [[CrossRef](#)]
48. Anwar, M.; Rasul, M.G.; Ashwath, N. A Systematic Multivariate Analysis of *Carica papaya* Biodiesel Blends and Their Interactive Effect on Performance. *Energies* **2018**, *11*, 2931. [[CrossRef](#)]
49. Yilmaz, I.T.; Gumus, M. Investigation of the effect of biogas on combustion and emissions of TBC diesel engine. *Fuel* **2017**, *188*, 69–78. [[CrossRef](#)]
50. Feroskhan, M.; Ismail, S.; Reddy, M.G.; Sai Teja, A. Effects of charge preheating on the performance of a biogas-diesel dual fuel CI engine. *Eng. Sci. Technol. Int. J.* **2018**, *21*, 330–337. [[CrossRef](#)]
51. Verma, S.; Das, L.M.; Kaushik, S.C.; Bhatti, S.S. The effects of compression ratio and EGR on the performance and emission characteristics of diesel-biogas dual fuel engine. *Appl. Therm. Eng.* **2019**, *150*, 1090–1103. [[CrossRef](#)]
52. Shan, X.; Qian, Y.; Zhu, L.; Lu, X. Effects of EGR rate and hydrogen/carbon monoxide ratio on combustion and emission characteristics of biogas/diesel dual fuel combustion engine. *Fuel* **2016**, *181*, 1050–1057. [[CrossRef](#)]
53. Rahman, K.A.; Ramesh, A. Studies on the effects of methane fraction and injection strategies in a biogas diesel common rail dual fuel engine. *Fuel* **2019**, *236*, 147–165. [[CrossRef](#)]
54. Barik, D.; Murugan, S. Experimental investigation on the behavior of a DI diesel engine fueled with raw biogas—Diesel dual fuel at different injection timing. *J. Energy Inst.* **2016**, *89*, 373–388. [[CrossRef](#)]

55. Ambarita, H. Performance and emission characteristics of a small diesel engine run in dual-fuel (diesel-biogas) mode. *Case Stud. Therm. Eng.* **2017**, *10*, 179–191. [[CrossRef](#)]
56. Sarkar, A.; Saha, U.K. Role of global fuel-air equivalence ratio and preheating on the behaviour of a biogas driven dual fuel diesel engine. *Fuel* **2018**, *232*, 743–754. [[CrossRef](#)]
57. Mohamed Ibrahim, M.; Varuna Narasimhan, J.; Ramesh, A. Comparison of the predominantly premixed charge compression ignition and the dual fuel modes of operation with biogas and diesel as fuels. *Energy* **2015**, *89*, 990–1000. [[CrossRef](#)]
58. Abdul Rahman, K.; Ramesh, A. Effect of reducing the methane concentration on the combustion and performance of a biogas diesel predominantly premixed charge compression ignition engine. *Fuel* **2017**, *206*, 117–132. [[CrossRef](#)]
59. Kalsi, S.S.; Subramanian, K.A. Effect of simulated biogas on performance, combustion and emissions characteristics of a bio-diesel fueled diesel engine. *Renew. Energy* **2017**, *106*, 78–90. [[CrossRef](#)]
60. Barik, D.; Murugan, S. Investigation on combustion performance and emission characteristics of a DI (direct injection) diesel engine fueled with biogas-diesel in dual fuel mode. *Energy* **2014**, *72*, 760–771. [[CrossRef](#)]
61. Bora, B.J.; Saha, U.K.; Chatterjee, S.; Veer, V. Effect of compression ratio on performance, combustion and emission characteristics of a dual fuel diesel engine run on raw biogas. *Energy Convers. Manag.* **2014**, *87*, 1000–1009. [[CrossRef](#)]
62. Tonkunya, N.; Wongwuttanasatian, T. Utilization of biogas-diesel mixture as fuel in a fertilizer pelletising machine for reduction of greenhouse gas emission in small farms. *Energy Sustain. Dev.* **2013**, *17*, 240–244. [[CrossRef](#)]
63. Park, S.H.; Yoon, S.H.; Cha, J.; Lee, C.S. Mixing effects of biogas and dimethyl ether (DME) on combustion and emission characteristics of DME fueled high-speed diesel engine. *Energy* **2014**, *66*, 413–422. [[CrossRef](#)]
64. Cacua, K.; Amell, A.; Cadavid, F. Effects of oxygen enriched air on the operation and performance of a diesel-biogas dual fuel engine. *Biomass Bioenergy* **2012**, *45*, 159–167. [[CrossRef](#)]
65. Sudheesh, K.; Mallikarjuna, J.M. Diethyl ether as an ignition improver for biogas homogeneous charge compression ignition (HCCI) operation—An experimental investigation. *Energy* **2010**, *35*, 3614–3622. [[CrossRef](#)]
66. Yoon, S.H.; Lee, C.S. Experimental investigation on the combustion and exhaust emission characteristics of biogas-biodiesel dual-fuel combustion in a CI engine. *Fuel Process. Technol.* **2011**, *92*, 992–1000. [[CrossRef](#)]
67. Lebedevas, S.; Pukalskas, S.; Daukšys, V.; Rimkus, A.; Melaika, M.; Jonika, L. Research on Fuel Efficiency and Emissions of Converted Diesel Engine with Conventional Fuel Injection System for Operation on Natural Gas. *Energies* **2019**, *12*, 2413. [[CrossRef](#)]
68. Szabados, G.; Bereczky, Á. Experimental investigation of physicochemical properties of diesel, biodiesel and TBK-biodiesel fuels and combustion and emission analysis in CI internal combustion engine. *Renew. Energy* **2018**, *121*, 568–578. [[CrossRef](#)]
69. Lijewski, P.; Fuc, P.; Dobrzynski, M.; Markiewicz, F. Exhaust emissions from small engines in handheld devices. *MATEC Web Conf. EDP Sci.* **2017**, *118*, 00016. [[CrossRef](#)]
70. Lijewski, P.; Merkisz, J.; Fuć, P.; Ziółkowski, A.; Rymaniak, Ł.; Kusiak, W. Fuel consumption and exhaust emissions in the process of mechanized timber extraction and transport. *Eur. J. For. Res.* **2017**, *136*, 153–160. [[CrossRef](#)]
71. Ogunkunle, O.; Ahmed, N.A. A review of global current scenario of biodiesel adoption and combustion in vehicular diesel engines. *Energy Rep.* **2019**, *5*, 1560–1579. [[CrossRef](#)]
72. Soam, S.; Hillman, K. Factors influencing the environmental sustainability and growth of hydrotreated vegetable oil (HVO) in Sweden. *Bioresour. Technol. Rep.* **2019**, *7*, 100244. [[CrossRef](#)]
73. Dabi, M.; Saha, U.K. Application potential of vegetable oils as alternative to diesel fuels in compression ignition engines: A review. *J. Energy Inst.* **2019**, *92*, 1710–1726. [[CrossRef](#)]
74. Bortel, I.; Vávra, J.; Takáts, M. Effect of HVO fuel mixtures on emissions and performance of a passenger car size diesel engine. *Renew. Energy* **2019**, *140*, 680–691. [[CrossRef](#)]
75. Suarez-Bertoa, R.; Kousoulidou, M.; Clairotte, M.; Giechaskiel, B.; Nuottimäki, J.; Sarjovaara, T.; Lonza, L. Impact of HVO blends on modern diesel passenger cars emissions during real world operation. *Fuel* **2019**, *235*, 1427–1435. [[CrossRef](#)]
76. Cheng, Q.; Tuomo, H.; Kaario, O.T.; Martti, L. Spray dynamics of HVO and EN590 diesel fuels. *Fuel* **2019**, *245*, 198–211. [[CrossRef](#)]

77. Di Iorio, S.; Magno, A.; Mancaruso, E.; Vaglieco, B.M. Analysis of the effects of diesel/methane dual fuel combustion on nitrogen oxides and particle formation through optical investigation in a real engine. *Fuel Process. Technol.* **2017**, *159*, 200–210. [[CrossRef](#)]
78. Li, Y.; Xu, H.; Cracknell, R.; Head, R.; Shuai, S. An experimental investigation into combustion characteristics of HVO compared with TME and ULSD at varied blend ratios. *Fuel* **2019**, *255*, 115757. [[CrossRef](#)]
79. Mansor, M.R.A.; Abbood, M.M.; Mohamad, T.I. The influence of varying hydrogen-methane-diesel mixture ratio on the combustion characteristics and emissions of a direct injection diesel engine. *Fuel* **2017**, *190*, 281–291. [[CrossRef](#)]
80. Verma, S.; Das, L.M.; Kaushik, S.C.; Tyagi, S.K. An experimental investigation of exergetic performance and emission characteristics of hydrogen supplemented biogas-diesel dual fuel engine. *Int. J. Hydrogen Energy* **2018**, *43*, 2452–2468. [[CrossRef](#)]
81. Vibe, I.I. Novoe o rabochem tsikle dvigatelei: Skorost' sgoraniia i rabochii tsikl dvigatel'ia [Новое рабочее цикле двигателей. Скорость сгорания и рабочий цикл двигателя.]. 1962. Available online: https://scholar.google.com.hk/scholar?hl=zh-TW&as_sdt=0%2C5&q=Novoe+o+rabochem+tsikle+dvigatelei%3A+Skorost%E2%80%99+sgoraniia+i+rabochii+tsikl+dvigatel'ia&btnG= (accessed on 2 January 2020).



© 2020 by the authors. Licensee MDPI, Basel, Switzerland. This article is an open access article distributed under the terms and conditions of the Creative Commons Attribution (CC BY) license (<http://creativecommons.org/licenses/by/4.0/>).